RSC Advances

PAPER

View Article Online
View Journal | View Issue

Cite this: *RSC Adv.*, 2016, **6**, 48523

A copper hexacyanocobaltate nanocubes based dopamine sensor in the presence of ascorbic acid

N. Karikalan,[a] M. Velmurugan,[a] S. M. Chen*[a] and K. Chelladurai[b]

Received 4th March 2016
Accepted 29th April 2016

DOI: 10.1039/c6ra05810h

www.rsc.org/advances

A novel copper hexacyanocobaltate based sensor was developed and its electrocatalytic behavior towards the oxidation of dopamine (DA) was demonstrated. Among the Prussian blue analogues, copper hexacyanocobaltate (CuHCC) exhibits unique electrochemical responses due to its bimetallic combination of copper and cobalt. As-prepared CuHCC shows a well-defined cubic structure with an average size of around 252 nm, which was confirmed by XRD and FE-SEM. Raman spectroscopy confirmed the coordination behavior of both the metal and ligand in CuHCC, which existed as Co^{III}–CN–Cu^{II} and Co^{II}–CN–Cu^{III}. The as-prepared CuHCC was used for the first time in DA detection and provided a better platform as a DA sensor. The electrocatalytic activity of CuHCC towards dopamine was examined by cyclic and differential pulse voltammetry. The CuHCC fabricated sensor shows a wide linear range from 0.1 to 350 μmol L^{-1} and low detection limit of 19 nmol L^{-1}. The sensor reported herein displays excellent sensitivity, high stability and appreciable reproducibility for DA oxidation.

1. Introduction

Dopamine (DA) is a neurotransmitter that plays a vital role in the central nervous system and peripheral nervous system.[1] Deficiency of DA in humans leads to Parkinson's disease, attention deficit hyperactivity disorder, schizophrenia and addiction.[2] In particular, Parkinson's disease, a degenerative disease of the nervous system shows symptoms of shivering, muscular rigidity, slow and imprecise movements.[3] Therefore, the determination of DA attains considerable importance in sensor applications.[4] Several methods have been employed to detect DA such as electrochemical, chromatography, colorimetry, fluorometry, chemiluminescence and electrophoresis.[5–10] Among all, electrochemical detection provides the foremost platform to quantify DA in real samples *via* its fast response and low cost systems. However, the strong influences of other interferents in physiological samples remains challenging, especially ascorbic acid (AA) and uric acid (UA) trespassing in real sample analysis.[11] Moreover, the high concentration of AA (0.2–0.5 mmol L^{-1}) in physiological samples significantly interfere with DA (10^{-8} to 10^{-6} mol L^{-1}).[12] Therefore, the desired materials are highly selective for the detection of DA in the presence of AA and UA because these analytes highly influence the determination of DA.[13] On the other hand, the materials should have a high electrochemical active area, stability, structural flexibility and biocompatibility.[14]

Recent studies have reported that carbonaceous materials and metal oxides manifest significant activity towards the nanomolar detection of DA.[15–17] Moreover, Prussian blue (PB) analogues have received remarkable attention in the sensors field due to their electron transport mechanism and controllable size.[18] The electrochemical properties of most metal hexacyanoferrates, such as NdHCF, AgHCF, SnHCF, CoHCF, NiHCF and CuHCF, have been extensively studied to date for the determination of AA, DA or UA.[19–24] These materials display excellent electrocatalytic activity towards AA, DA and UA with selective and simultaneous performance. However, to the best of our knowledge, metal hexacyanocobaltates based materials have not been evaluated comprehensively. Moreover, copper based compounds exhibit reasonable performance towards DA detection, particularly the oxides of copper.[25] Previously, copper and cadmium hexacyanocobaltate have been studied towards carcinoembryonic antigen (CEA), alpha-fetoprotein (AFP) and RNA detection.[26] These reports concluded that the hexacyanocobaltate based materials were a sensitive substrate for biomolecules detection.

Therefore, in the present study we have concentrated on copper hexacyanocobaltate ($Cu_3[Co(CN)_6]_2$) for the selective detection of DA oxidation in the physiological pH range (pH 7.2). Furthermore, the cubic crystal morphology of CuHCC was characterized by FESEM, XRD and Raman spectroscopy. To the best our knowledge, this is the first report on the electrochemical behaviour of CuHCC towards DA oxidation. In addition, the selectivity of CuHCC is well appreciated towards DA oxidation in the presence of strong interferents such as AA and UA. Moreover, the performance of CuHCC was demonstrated in

[a]*Electroanalysis and Bioelectrochemistry Lab, Department of Chemical Engineering and Biotechnology, National Taipei University of Technology, No. 1, Section 3, Chung-Hsiao East Road, Taipei 106, Taiwan, Republic of China. E-mail: smchen78@ms15.hinet.net ; Fax: +886-2-27025238; Tel: +886-2-27017147*

[b]*Department of Chemistry, National Taiwan University, Taipei 106, Taiwan, Republic of China*

real samples such as dopamine injection, urine, blood and blood serum. The nanomolar detection of DA on CuHCC/GCE was evaluated using voltammetric methods. The electrocatalytic range of DA oxidation on CuHCC/GCE was from 0.1 to 350 μmol L^{-1}. The fabricated sensor was able to sense a minimum level of DA of around 19 nmol L^{-1}. The proposed sensor is a highly sensitive substrate for DA sensing when compared to other Prussian blue analogues.

2. Experimental

2.1. Materials

Potassium hexacyanocobaltate ($K_3(Co(CN)_6)$), copper chloride dihydrate ($CuCl_2 \cdot 2H_2O$), dopamine, uric acid, ascorbic acid, potassium hydrogen phosphate and dihydrogen phosphate were obtained from Aldrich chemical Co. and used as received.

2.2. Apparatus

The X-ray diffraction patterns of the compounds studied were performed using a XRD, XPERT-PRO spectrometer (PANalytical B.V., The Netherlands) with CuK_α radiation (λ = 1.5406 Å). FESEM images were obtained using a FEG QUANTA 250 microscope. Raman spectroscopy was carried out using an NT-MDT, NTEGRA SPECTRA spectrometer. A CHI 1205B electrochemical analyzer (CH Instruments, USA) was used to perform cyclic voltammetry and chronoamperometry. Differential pulse voltammetry (DPV) measurements were performed using a CHI 900 apparatus (CH Instruments, USA). A conventional three electrode system was employed for the catalysis comprising a glassy carbon working electrode (0.07 cm^2), platinum wire auxiliary electrode and Ag/AgCl/3 M KCl reference electrode.

2.3. Synthesis and fabrication of CuHCC for the DA sensor

The described material was synthesized *via* precipitation method, wherein potassium hexacyanocobaltate ($K_3(Co(CN)_6)$) was added to copper chloride dihydrate ($CuCl_2 \cdot 2H_2O$). In this method, we used a 3 : 2 ratio of metal and complex ligand; this furnishes the compound without potassium in its lattice. Herein, 300 mL of 0.05 M $CuCl_2 \cdot 2H_2O$ was added to 200 mL of 0.05 M ($K_3(Co(CN)_6)$). The solution suddenly turns to colloids of a sky blue color mixture of $Cu_3[Co(CN)_6]_2$ crystals and this mixture was maintained under vigorous stirring conditions for an hour. Finally, the compound was collected by centrifugation and washed several times with Milli-Q (18 MΩ) water and dried in an oven overnight at 45 °C. Subsequently, the sample was stored in a closed container to avoid moisture and named as CuHCC. To fabricate the CuHCC modified electrode, the CuHCC was re-dispersed in Mill-Q water at about 5 mg mL^{-1} and further sonicated for 10 min to obtain a uniform suspension. About 8 μL of this suspension was drop cast on a GCE and then dried at 50 °C for stable film formation. The successfully fabricated sensor material can be used in the DA sensor. A screen-printed carbon electrode (SPCE) was used as a disposable sensor electrode. We have modified the SPCE with CuHCC and directly applied it towards dopamine determination. The CuHCC disposable DA sensor is shown in Scheme 1.

3. Results and discussion

3.1. Characterization of CuHCC

The hexacyanometalates form zeolitic compounds with transition metals, mainly Prussian blue, which has been studied extensively. The common formula of the Prussian blue analogue is $A_xM_y[M(CN)_6]_z \cdot nH_2O$ (where A = alkali metal cation, M = transition metal cation and either are the same or different). The crystal model of $Cu_3[Co(CN)_6]_2$ is shown in Fig. 1 in which Cu^{2+} is high-spin state coordinated with N and Co^{3+} is in the low-spin state and coordinated with C. In general, the metal ions share the edge site of the cube and the cyanide ions bridge the metal ions.[27] The electronic structure and coordination sites of $Cu_3[Co(CN)_6]_2$ were analyzed by Fourier transform infrared (FT-IR) and Raman spectroscopy.

As shown in Fig. 2(a), the FT-IR results provide information on the octahedral $Co(CN)_6$ ligand, wherein the observed absorption bands were related to the vibrations of –CN, Co–C and water.[28] In this crystal lattice, water molecules occupy the zeolitic site, which was clearly inferred from the FT-IR stretching and bending vibrations at around 3435 and 1604 cm^{-1}; usually, the former peak appears as a sharp band but here it was broad due to the movement of hydrogen bonded water.[29] Commonly, all hexacyanocobaltate shows the vibration around 430–470 cm^{-1}, this sharp peak shows the bonding information for Co–C in $Co(CN)_6$. Finally, the stretching frequency around 2189 cm^{-1} confirms the –CN bridging between two metals; among the transition metal cobalt cyanides copper reveals a higher stretching frequency due to strong bonding between Cu and N.[30] The cyanide ion bridging is familiar in the hexacyanometalates wherein it was coordinated to the metal by both sides of the cyanide ion (*i.e.*, the carbon end and nitrogen end). On the carbon side, the cyanide ion acts as a strong ligand and therefore it makes a low-spin configuration towards metals. Conversely, the nitrogen side will act as a weak ligand compared to carbon so it makes a high-spin configuration towards metals. However, different oxidation states are possible in $M^{\delta+}$–C≡N–$M^{\delta+}$ coordination such as Co^{II}–CN–Cu^{II}, Co^{III}–CN–Cu^{II}, Co^{II}–CN–Cu^{III} and Co^{III}–CN–Cu^{III}.

Raman spectroscopy is a useful tool used to assess the different valance states. Fig. 2(b) depicts the Raman spectrum of CuHCC wherein the peaks observed at 2200 and 2218 cm^{-1}

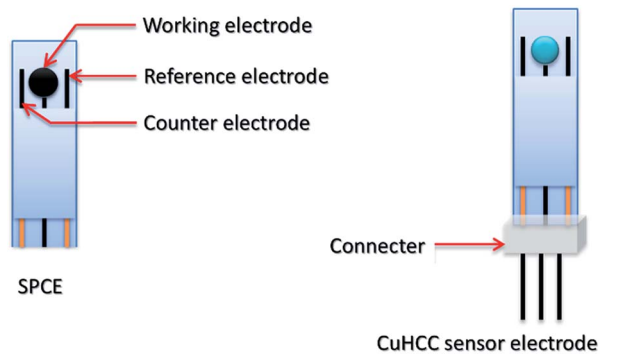

Scheme 1 The proposed design of final device for dopamine sensor electrode modified by CuHCC nanocubes.

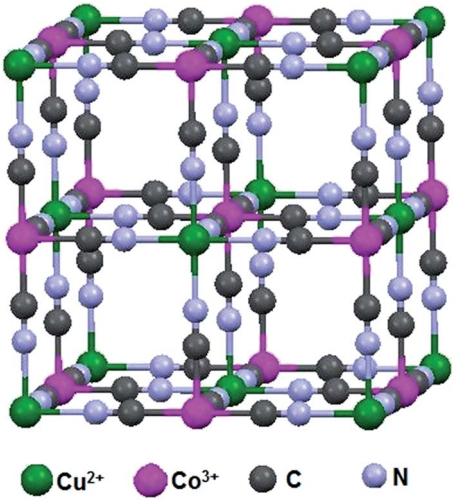

Fig. 1 Schematic of the copper hexacyanocobaltate lattice structure.

correspond to cyanide ion stretching. The two peaks are merged and pronounced on the broad peak, herein the frequencies at 2088 and 2134 cm^{-1} were attributed to the Co^{III}–CN–Cu^{II} and Co^{II}–CN–Cu^{III}, these results confirm the mixture of mixed valance states present in the compound.

The structural behavior of CuHCC was studied by powder X-ray diffraction (Fig. 2(c)). Previously, A. Ratuszna and G. Małecki established the XRD patterns of CuHCC,[48] which closely matched with the as-prepared compound CuHCC, which crystallizes in the $Fm\bar{3}m$ space group with $a = 10.49$ Å. The peaks observed at, 25.3°, 29.7°, 36.0°, 40.6°, 44.8°, 51.8°, 55.6°, 58.8°, 68.1° and 70.9° were attributed to (200), (220), (311), (400), (420), (422), (440), (600), (620), (640) and (642) planes, respectively. These peaks reveal that the compound was highly crystalline in nature and the rough baselines indicate some of crystals being squeezed or crushed. The predominant peak observed at 17.8° corresponds to the (200) plane, which denotes most of the compound was exposed in this plane and therefore the crystallite size was calculated from this plane using the Debye–Scherrer formula. The calculated crystallite size was 278 nm for this plane and the average crystallite size was 252 nm. Most of the Prussian blue analogues disclose a discrete cubic structure with an average particle size of 70–700 nm.[31–34] CuHCC also shows a cubic structure, which was further confirmed by FE-SEM, as shown in Fig. 2(d). CuHCC exhibited uniformly distributed cubes with a distinct boundary with an average particle size of 250–280 nm, which was matched with calculated crystallite size (calculated from the XRD analysis).

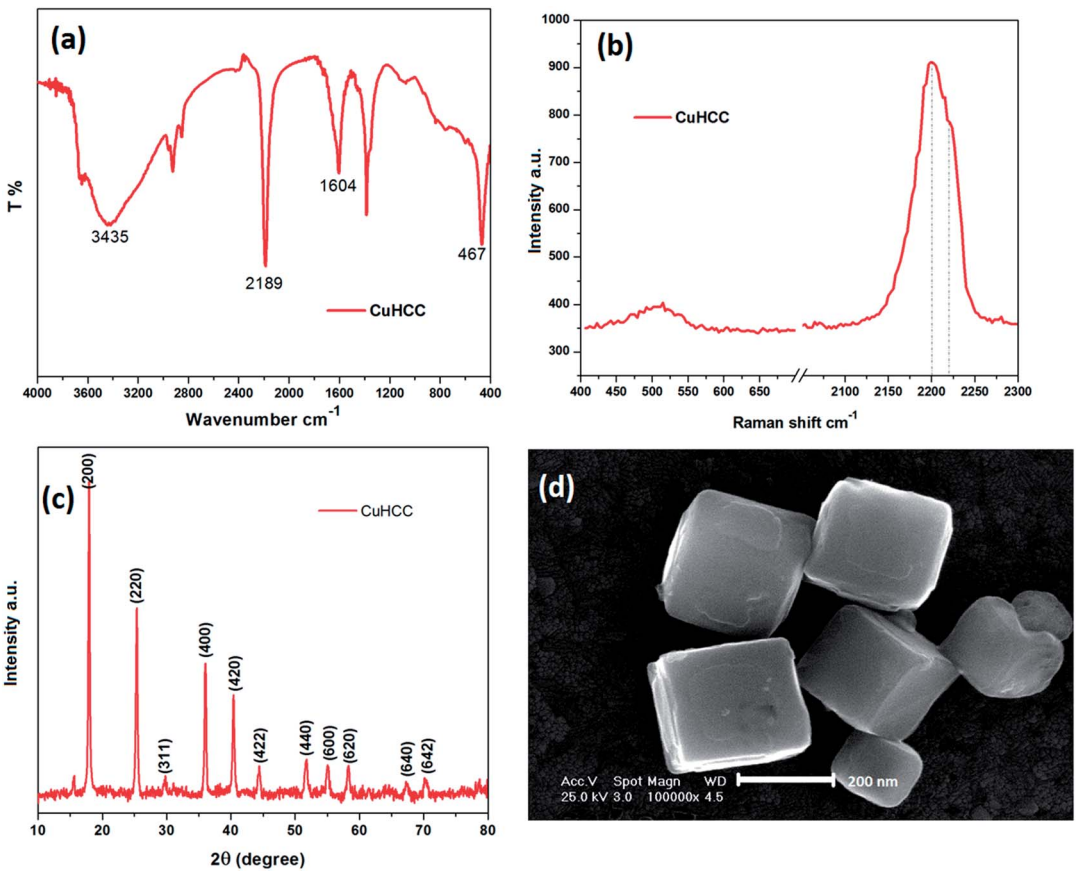

Fig. 2 (a) FT-IR spectra, (b) Raman spectra, (c) powder XRD patterns and (d) FE-SEM images of the as-prepared CuHCC.

3.2. The electrocatalytic oxidation of dopamine

The electrocatalytic behavior of CuHCC was studied towards the electro-oxidation of DA. Fig. 3(a) shows the cyclic voltammetry (CV) responses of bare and CuHCC modified GCEs in 100 μmol L^{-1} DA containing 0.1 M phosphate buffer solution (PBS, pH 7.2) at a scan rate of 50 mV s^{-1}. A pair of quasi-reversible peaks was obtained for both electrodes; however, the bare GCE reveals better curvature for both the anodic and cathodic peaks. Other than bare GCE, most carbonaceous materials exhibit a strong quasi-reversible peak for dopamine oxidation. The anodic (E_{pa}) and cathodic (E_{pc}) peak potential of the bare and CuHCC modified GCEs were 0.35 V, 0.22 V and 0.07 V, 0.07 V, respectively. The peak-to-peak separation was found to be 280 mV for the bare GCE, whereas the CuHCC modified electrode exhibited only 150 mV because of the low onset potential (oxidation) of the CuHCC modified electrode. Moreover, the oxidation peak current of DA was five times higher for the CuHCC modified electrode when compared to the bare GCE. The reason is the bi-metallic nature of CuHCC provides suitable binding sites (Co–CN–Cu) for DA wherein it can be easily adsorbed on the surface of the CuHCC modified electrode. Moreover, the low spin configuration of Co^{3+} (d^6) was stable in the lattice by the completely filled t_{2g} orbital; moreover, the high spin configuration of Cu^{2+} (d^9) remains unstable due to the vacant orbital. Therefore, it needs one electron to achieve its fully occupied orbital configuration and therefore it oxidizes DA with the aid of Co^{3+}. However, to recover the lattice geometry, K^+ ions are inserted into the lattice (from the electrolyte) and reduce Co^{3+} to Co^{2+} (see the mechanism in Scheme 2). Fig. 3(a) (inset) depicts the CV responses of the bare and CuHCC modified GCEs in the absence of DA, wherein the CuHCC modified electrode exhibits a high capacitive background current and a reduction peak at 0.14 V *vs.* Ag/AgCl (onset potential) when compared to the bare GCE. This value suggests that the as-prepared compound performed well when compared with the bare GCE.

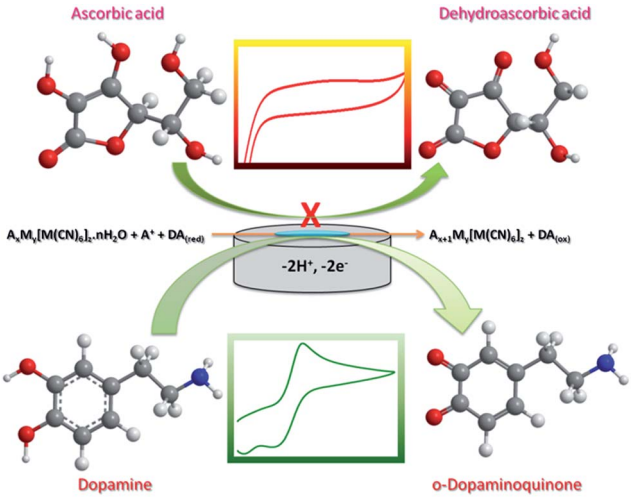

Scheme 2 The possible mechanism for the detection of DA and the electrochemical response of AA on the CuHCC modified electrode.

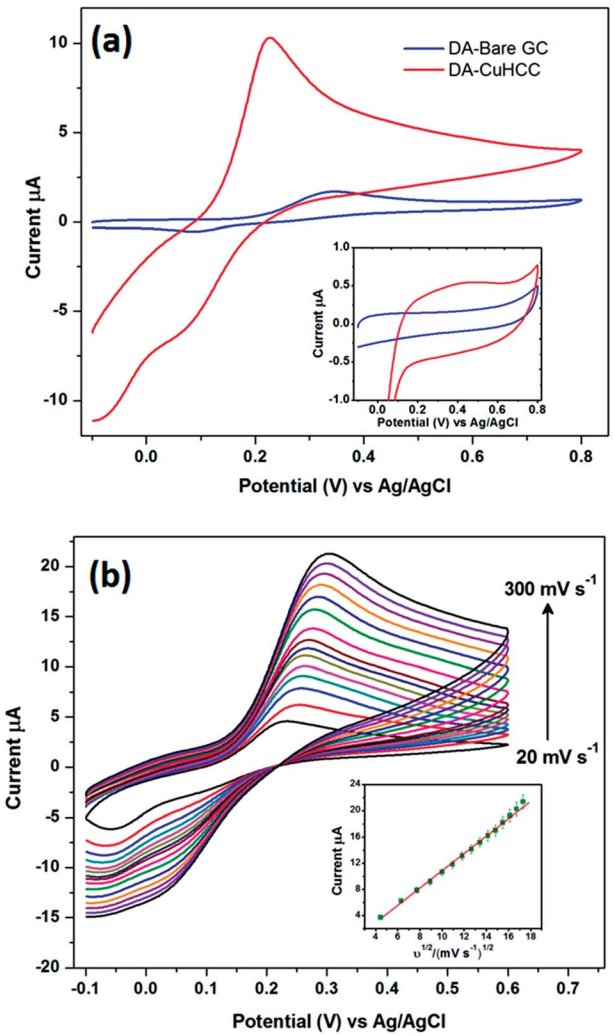

Fig. 3 (a) CVs recorded for 100 μmol L^{-1} DA at the bare GCE (blue) and CuHCC modified GCE (red) at a scan rate of 50 mV s^{-1}. The inset shows the CVs obtained in the absence of DA at the bare GCE and CuHCC modified GCE in 0.1 mol L^{-1} PBS (pH 7.2) at a scan rate of 50 mV s^{-1}. (b) The CV of the CuHCC modified GCE in 100 μmol L^{-1} DA containing 0.1 mol L^{-1} PBS at different scan rates from 20 to 300 mV s^{-1}. The inset shows the plot of I_{pa} *vs.* $\nu^{1/2}$.

3.3. The effect of the scan rate

The effect of the scan rate was investigated for the CuHCC modified electrode in 100 μmol L^{-1} DA containing 0.1 M PBS using CV at a scan rate of 50 mV s^{-1}, as shown in Fig. 3(b). The redox peak current of DA oxidation linearly increases upon increasing the scan rate from 20 to 300 mV s^{-1}. However, the redox peak potential slightly shifts towards the positive and negative side for the anodic and cathodic reactions, respectively. This is due to the increase in internal resistance caused by increasing the DA concentration; herein, DA adsorbs on the electrode surface and forms a thin layer (unreal), which restricts bulk electrolyte movement from the bulk solution to the diffusion layer (inner and outer Helmholtz plane). The anodic peak current (I_{pa}) of DA oxidation was plotted against the square root of the scan rate, as shown in Fig. 3(b) (inset), which follows the

good linearity with a correlation coefficient of 0.9966. The cathodic peak current (I_{pc}) was interfering with the compound's reduction peak; therefore, this peak was merged with the cathodic peak of DA oxidation upon increasing the scan rate. Therefore, we acquired only the anodic peak on this account and we confirmed the DA oxidation was fully controlled by a diffusion process using this plot.

3.4. Determination of dopamine

Differential pulse voltammetry (DPV) provides a highly sensitive current and better detection when compared to CV and therefore the determination of DA was carried out using DPV. Fig. 4 depicts the DPV responses of the CuHCC modified electrode for the addition of different concentrations of DA from 0.1 to 650 μmol L^{-1}. It can be observed that a sharp DPV response was observed for the addition of 0.1 μmol L^{-1} DA and the current response increased linearly upon increasing the concentration of DA. The DPV response of the CuHCC modified electrode was linear over the concentration range of 0.1–350 μmol L^{-1} (Fig. 4 (inset)) with a correlation coefficient R^2 = 0.9954. This study stated that the highest linear range of 0.1–350 μmol L^{-1} and lower limit detection (LOD) of 0.019 μmol L^{-1} was achieved by the CuHCC towards the detection of DA. The performance of the fabricated sensor was compared with recently reported DA sensors and the comparative results shown in Table 1. In addition, the CuHCC nanocubes modified electrode was also compared with other copper nanostructures (nanoparticles, nanoleaf, nanocubes and microspheres) based DA sensors (see Table 1). The analytical comparison of our proposed sensor clearly reveals that the CuHCC nanocubes modified electrode has a low LOD and better linear range for the detection of DA when compared to the other modified electrodes. The mechanism and superior performance of the CuHCC modified electrode was elaborately explained in above section.

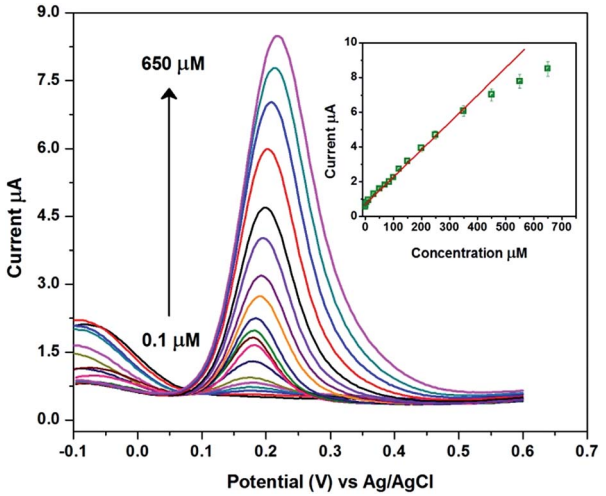

Fig. 4 The DPV of the CuHCC modified electrode for the addition of different concentrations of DA from 0.1 to 650 μmol L^{-1}. The inset shows the calibration plot of current *vs.* concentration (0.1 to 650 μmol L^{-1}).

3.5. The effect of interference and selectivity

AA, DA and UA play vital roles in human health and it is well known that electrochemically they are responsive with close potential differences.[43] Therefore, the determination of DA in the presence of AA and DA is quite important. Electrochemical detection of these compounds has more interest but some cases AA highly interferes with DA. Commonly, AA co-exists with DA in bodily fluids and is also present at higher concentrations when compared with DA. Herein, we demonstrated the selective detection of DA by the CuHCC modified electrode in the presence of AA and UA in PB with a 100-fold and 10-fold excess of AA and UA, respectively when compared to DA. Fig. 5(a) shows the CVs of DA oxidation in the presence of the different interfering analytes, such as AA and UA, wherein AA does not interfere with

Table 1 A comparison of the performance of DA oxidation between CuHCC/GCE and other modified electrodes

Electrode	Electrolyte	Method	Linear range, μmol L^{-1}	Detection limit, μmol L^{-1}	Ref.
Graphene/GCE	PBS (pH 7)	DPV	4–100	2.64	37
TiO_2/graphene/GCE	PBS (pH 7)	DPV	5–200	2	38
SZP/MB	Tris–HCl (pH 7.4)	DPV	6–100	1.7	39
CuO/MWNTs/Nafion/GCE	PBS (pH 6)	DPASV	1.0–80	0.4	35
SWCNT/Fe_2O_3/GCE	PBS (pH 7)	SWV	3.2–31.8	0.36	40
GO/GCE	B–R (pH 5)	DPV	1.0–15	0.27	12
Pt/RGO/MnO_2/GCE	PBS (pH 7)	DPV	1.5–215.56	0.1	11
CuO/CPE	PBS (pH 6)	DPV	0.3–1.4, 2–20	0.055	36
MnO_2/chitosan/AuE	KNO_3 (pH 4 to 9)	CA	0.10–12.0	0.04	41
γ-WO_3/GCE	PBS (pH 7)	DPV	0.1–50, 50–600	0.024	13
NiHCF/PNH/AuE	PBS (pH 7)	DPV	0.1–4.3, 4.3–9.6	0.021	23
CHI/VSG/PPy scaffold	PBS (pH 6)	DPV	0.1–200	0.0194	42
Cu nanocubes/GCE	PBS (pH 6.5)	CA	0.5–300, 300–2000	0.2	44
		DPV	0.001–0.1, 0.5–200	0.002	
Cu_2O HMS/CB/GCE	PBS (pH 5.7)	CA	0.099–708	0.0396	45
CuO nanoleaf	PBS (pH 8)	DPV	1–7.5, 7.5–140	0.5	46
ZnO nanorod/flower like CuO/AuE	PBS (pH 7.3)	CA	1000–8000	100	47
CuHCC nanocubes/GCE	PBS (pH 7.2)	DPV	0.1–350	0.019	This work

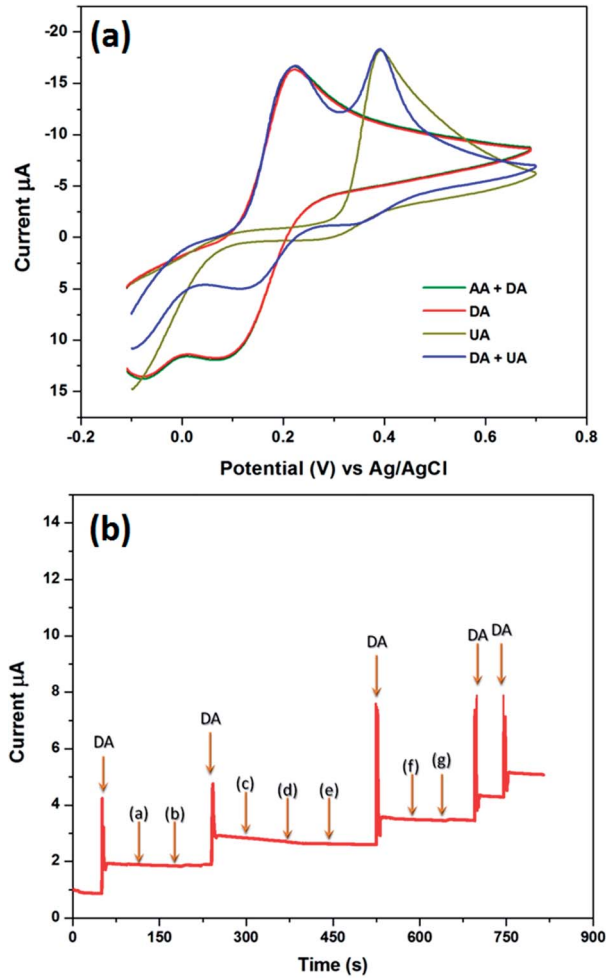

Fig. 5 (a) The CVs of the CuHCC modified electrode in the presence of AA and UA in DA containing PBS (pH 7.2) with a 100-fold and 10-fold excess of AA and UA, respectively. (b) The chronoamperometric response of the CuHCC modified electrode upon the addition of 100 µmol L^{-1} DA with the addition of the interferents: (a) NaCl, (b) KCl, (c) epinephrine, (d) norepinephrine, (e) serotonin, (f) glucose and (g) L-tyrosine in 0.1 mol L^{-1} PBS (pH 7.2); applied potential = 0.2 V (Ag/AgCl).

Table 2 The determination of DA oxidation in diluted dopamine hydrochloride injections using the CuHCC modified GCE

Sample	Added (µmol L^{-1})	Detected[a] (µmol L^{-1})	Recovery (%)	RSD[b] (%)
1	5	5.11	102.2	2.1
2	10	9.89	98.9	1.6
3	20	19.96	99.8	1.9

[a] Standard addition method. [b] Relative standard deviation for three measurements.

DA oxidation. This is clearly inferred from Fig. 5(a); the DA and AA mixture exhibit current responses merged over the DA oxidation curve. Therefore, there is no electrocatalytic response observed for AA and this may be due to the negatively charged nature of AA (pK_a = 4.10) at pH 7.0, whereas DA is positively charged (pK_a = 8.87) at physiological pH (7.2 to 7.4). According to crystal field theory, the strong ligands donate their charges to metal ions and therefore will acquire a negative charge. Therefore, the negative charge of the metal ions provides the space for DA adsorption (positively charged nature). At the same time it repels the negatively charged AA. Therefore, the protonated DA was simply adsorbed on the surface of the CuHCC modified electrode and oxidized, which manifests a large oxidative current response (Scheme 2). On the other hand, the CuHCC modified electrode also oxidizes UA; however, it comes at a different potential with a sharp peak current. However, the electrocatalytic performance of UA was not much better compared with previous reports, so the present study only concentrates on the detection of DA.

Table 3 The determination of DA in diluted biological samples using the CuHCC nanocubes modified GCE

Biological samples	Added (µmol L^{-1})	Detected[a] (µmol L^{-1})	Recovery (%)	RSD[b] (%)
Blood	10	9.68	96.8	3.2
Blood serum	10	9.94	99.4	1.8
Urine	10	9.82	98.2	2.8

[a] Standard addition method. [b] Relative standard deviation for three measurements.

Apart from AA and UA, other biological interference can also affect DA oxidation; however, AA and UA are essential. We also analyzed other interference such as NaCl, KCl, epinephrine, norepinephrine, serotonin, glucose and L-tyrosine. Fig. 5(b) depicts the chronoamperometric responses of DA oxidation with the various interferents, wherein the fabricated sensor would selectively oxidize DA in the presence of the other interferents in high concentrations.

3.6. Determination of DA in real samples

To study the practicability of the CuHCC fabricated sensor in real sample analysis, a dopamine hydrochloride injection was explored. A stock solution of DA injection sample was made *via* appropriate dilution with 0.1 M PBS (pH 7.2) and used for the detection of DA. The recovery of DA was calculated using the standard addition method, as reported previously. The obtained recoveries of DA are summarized in Table 2 and the recoveries were in the range of 98.9–102.2%. The results confirmed that the proposed CuHCC modified electrode has appropriate recovery towards DA and could be used for real time sensing of DA in pharmaceutical formulations. In addition, we have analysed the DA in other real samples (urine, blood and blood serum) and gathered appropriate recoveries that are given in Table 3. We have provided the design of the final device that can be used for miniature applications (Scheme 1).

4. Conclusions

In summary, a novel CuHCC modified electrode has been used for the sensitive, selective and lower overpotential detection of DA. The CuHCC modified electrode exhibited a wider linear range (0.1–350 µmol L^{-1}) and lower LOD (19 nmol L^{-1}) for DA

when compared to the Prussian blue analogues modified electrodes previously reported. The proposed sensor has high selectivity towards DA in the presence of an excess amount of UA, AA and other neurotransmitters. The good recovery of DA in commercial dopamine injection samples further authenticates that the CuHCC modified electrode can be used for the precise detection of DA in pharmaceutical formulations.

Acknowledgements

This project was supported by the National Science Council and the Ministry of Education of Taiwan, ROC.

Notes and references

1 M. Liu, L. Wang, J. Deng, Q. Chen, Y. Li, Y. Zhang, H. Li and S. Yao, *Analyst*, 2012, **137**, 4577.
2 C. Karuppiah, S. Sakthinathan, S. M. Chen, K. Manibalan, S. M. Chen and S. T. Huang, *Appl. Organomet. Chem.*, 2016, **30**, 40.
3 H. Shimura, N. Hattori, S. Kubo, Y. Mizuno, S. Asakawa, S. Minoshima, N. Shimizu, K. Iwai, T. Chiba, K. Tanaka and T. Suzuki, *Nat. Genet.*, 2000, **25**, 302.
4 R. M. Wightman, J. M. Leslie and C. M. Adrian, *Anal. Chem.*, 1988, **60**, 769A.
5 S. R. Ali, Y. Ma, R. R. Parajuli, Y. Balogun, W. Y. C. Lai and H. He, *Anal. Chem.*, 2007, **79**, 2583.
6 C. L. Guan, J. Ouyang, Q. L. Li, B. H. Liu and W. R. G. Baeyens, *Talanta*, 2000, **50**, 1197.
7 H. P. Wu, T. L. Cheng and W. L. Tseng, *Langmuir*, 2007, **23**, 7880.
8 L. L. Li, H. Y. Liu, Y. Y. Shen, J. R. Zhang and J. J. Zhu, *Anal. Chem.*, 2011, **83**, 661.
9 Y. Ma, M. Zhao, B. Cai, W. Wang, Z. Ye and J. Huang, *Chem. Commun.*, 2014, **50**, 11135.
10 J. Wang, M. P. Chatrathi, B. Tian and R. Polsky, *Anal. Chem.*, 2000, **72**, 2514.
11 B. Yang, J. Wang, D. Bin, M. Zhu, P. Yang and Y. Du, *J. Mater. Chem. B*, 2015, **3**, 7440.
12 F. Gao, X. Cai, X. Wang, C. Gao, S. Liu, F. Gao and Q. Wang, *Sens. Actuators, B*, 2013, **186**, 380.
13 A. C. Anithaa, N. Lavanya, K. Asokan and C. Sekar, *Electrochim. Acta*, 2015, **167**, 294.
14 V. Hariharan, S. Radhakrishnan, M. Parthibavarman, R. Dhilipkumar and C. Sekar, *Talanta*, 2011, **85**, 2166.
15 A. Yang, Y. Xue, Y. Zhang, X. Zhang, H. Zhao, X. Li, Y. He and Z. Yuan, *J. Mater. Chem. B*, 2013, **1**, 1804.
16 J. Liu, Z. He, J. Xue and T. T. Y. Tan, *J. Mater. Chem. B*, 2014, **2**, 2478.
17 P. Gai, H. Zhang, Y. Zhang, W. Liu, G. Zhu, X. Zhang and J. Chen, *J. Mater. Chem. B*, 2013, **1**, 2742.
18 S. S. Kaye and R. L. Jeffrey, *J. Am. Chem. Soc.*, 2005, **127**, 6506.
19 Q. L. Sheng, H. Yu and J. B. Zheng, *Electrochim. Acta*, 2007, **52**, 4506.
20 M. Noroozifar, M. K. Motlagh and A. Taheri, *Talanta*, 2010, **80**, 1657.
21 R. Hosseinzadeh, R. E. Sabzi and K. Ghasemlu, *Colloids Surf., B*, 2009, **68**, 213.
22 Z. Xun, C. Cai, W. Xing and T. Lu, *J. Electroanal. Chem.*, 2003, **545**, 19.
23 M. H. Mashhadizadeh, T. Yousefi and A. N. Golikand, *Electrochim. Acta*, 2012, **59**, 321.
24 R. Pauliukaite, M. E. Ghica and C. M. A. Brett, *Anal. Bioanal. Chem.*, 2005, **381**, 972.
25 F. Zhang, Y. Li, Y. Gu, Z. Wang and C. Wang, *Microchim. Acta*, 2011, **173**, 103.
26 Z. Wang, X. Chen and Z. Ma, *Biosens. Bioelectron.*, 2014, **61**, 562.
27 P. Zhou, D. Xue, H. Luo and X. Chen, *Nano Lett.*, 2002, **2**, 845.
28 C. P. Krap, B. Zamora, L. Reguera and E. Reguera, *Microporous Mesoporous Mater.*, 2009, **120**, 414.
29 J. Roque, E. Reguera, J. Balmaseda, J. Rodrıguez-Hernandez, L. Reguera and L. F. del Castillo, *Microporous Mesoporous Mater.*, 2007, **103**, 57.
30 J. T. R. Dunsmuir and A. P. Lane, *J. Chem. Soc. A*, 1971, 776.
31 M. Hu, N. L. Torad and Y. Yamauchi, *Eur. J. Inorg. Chem.*, 2012, **2012**, 4795.
32 Y. Huang, L. Hu, T. Zhang, H. Zhong, J. Zhou, Z. Liu, H. Wang, Z. Guo and Q. Chen, *Sci. Rep.*, 2013, **3**, 2647.
33 L. Hu, J. Mei, Q. Chen, P. Zhang and N. Yan, *Nanoscale*, 2011, **3**, 4270.
34 S. Vaucher, J. Fielden, M. Li, E. Dujardin and S. Mann, *Nano Lett.*, 2002, **2**, 225.
35 S. Yang, G. Li, Y. Yin, R. Yang, J. Li and L. Qu, *J. Electroanal. Chem.*, 2013, **703**, 45–51.
36 S. Reddy, B. E. K. Swamy and H. Jayadevappa, *Electrochim. Acta*, 2012, **61**, 78.
37 Y. R. Kim, S. Bong, Y. J. Kang, Y. Yang, R. K. Mahajan, J. S. Kim and H. Kim, *Biosens. Bioelectron.*, 2010, **25**, 2366.
38 Y. Fan, H. T. Lu, J. H. Liu, C. P. Yang, Q. S. Jing, Y. X. Zhang, X. K. Yang and K. J. Huang, *Colloids Surf., B*, 2011, **83**, 78.
39 J. Arguello, V. L. Leidens, H. A. Magosso, R. R. Ramos and Y. Gushikem, *Electrochim. Acta*, 2008, **54**, 560.
40 A. S. Adekunle, B. O. Agboola, J. Pillay and K. I. Ozoemena, *Sens. Actuators, B*, 2010, **148**, 93.
41 Y. Huang, C. Cheng, X. Tian, B. Zheng, Y. Li, H. Yuan, D. Xiao and M. F. Martin Choi, *Electrochim. Acta*, 2013, **89**, 832.
42 J. Liu, H. Ziming, J. Xue and T. T. Y. Tan, *J. Mater. Chem. B*, 2014, **2**, 2478.
43 L. Yang, D. Liu, J. Huang and T. You, *Sens. Actuators, B*, 2014, **193**, 166.
44 B. Luo, X. Li, J. Yang, J. Gu, M. Wang and L. Jiang, *ECS Electrochem. Lett.*, 2014, **3**, B5–B7.
45 L. N. Wu, Y. L. Tan, L. Wang, S. N. Sun, Z. Y. Qu, J. M. Zhang and Y. J. Fan, *Microchim. Acta*, 2015, **182**, 1361.
46 Z. Zheng, H. Qiu, M. Zheng, S. Weng, Z. Huang, R. Xian and X. Lin, *Anal. Methods*, 2014, **6**, 7923.
47 K. Khun, Z. H. Ibupoto, X. Liu, N. A. Mansor, A. P. F. Turner, V. Beni and M. Willander, *J. Nanosci. Nanotechnol.*, 2014, **14**, 6646.
48 G. Małecki and A. Ratuszna, *Powder Diffr.*, 1999, **14**, 25.